# Hidden periodicity in LiDAR point-count rasters

A. Urias

**Author:** A. Urias, Independent Researcher, Hermosillo, Sonora, Mexico. **ORCID:** https://orcid.org/0009-0007-3147-323X. **Email:** alexurias@gmail.com

**Preprint status:** This is a non-peer reviewed preprint submitted to EarthArXiv.

**Keywords:** LiDAR; LAS format; point density; rasterization; quantization; aliasing; spectral analysis

## Abstract

LAS files store coordinates on a fixed step, usually 1 cm, and counting points in raster cells can add a regular pattern that comes from the storage and counting grids rather than the ground. We ask how a user can test whether a repeating pattern in a point-count raster was introduced this way. We model three mechanisms (grid mismatch, boundary rounding and uneven filling of stored positions), predict their size and, for grid mismatch, where they appear in a spectrum, and test the predictions with controlled changes on UAV, mobile and airborne point clouds and in PDAL and lidR. Stripe sizes matched the predictions (median regression slope 1.00), and moving a 10 cm grid by 5 mm reduced the RMS relative count change per cell of a UAV raster from 11.6 % to 0.5 %. In an airborne tile where the pattern was more than 30 times weaker than the counting noise of one cell, its spectral lines stood well above the spectral background, and random thinning showed the expected rise of line-to-background ratio with the square root of the number of points. Across eight cell sizes the grid-mismatch line followed its predicted ground wavelength while a reference component stayed fixed. The effects are largest for cells below a few decimetres. Because each mechanism responds to a different controlled change, a suspicious pattern can be tested, and each mechanism has its own remedy.

## 1. Introduction

Point-count rasters are routine LiDAR products, used for density checks, ecological metrics and classifier inputs. Figure 1a shows PDAL counts of a UAV survey in 10 cm cells after its coordinates were rounded to 1 cm, divided by the counts of the same points from their original 0.1 mm coordinates. The ratio measures how rounding changed each cell's count relative to that finer reference; some change is expected where rounding moves points across a boundary, but the map shows a regular crosshatch with an RMS of 11.6 %. Moving the grid by 5 mm (Fig. 1b) reduces it to 0.5 %. Both values are for the whole 40 m crop. The squared map RMS is the sum of the squared easting stripe, northing stripe and cell-level residual, so the map RMS exceeds the one-axis profile stripes reported later. In the 6 m window shown in Fig. 1a the map RMS is 11.9 %: an easting stripe of 6.4 %, a northing stripe of 6.4 % and a cell-level residual of 7.7 % that neither profile captures; the 5 mm shift brings the window to 0.6 %.

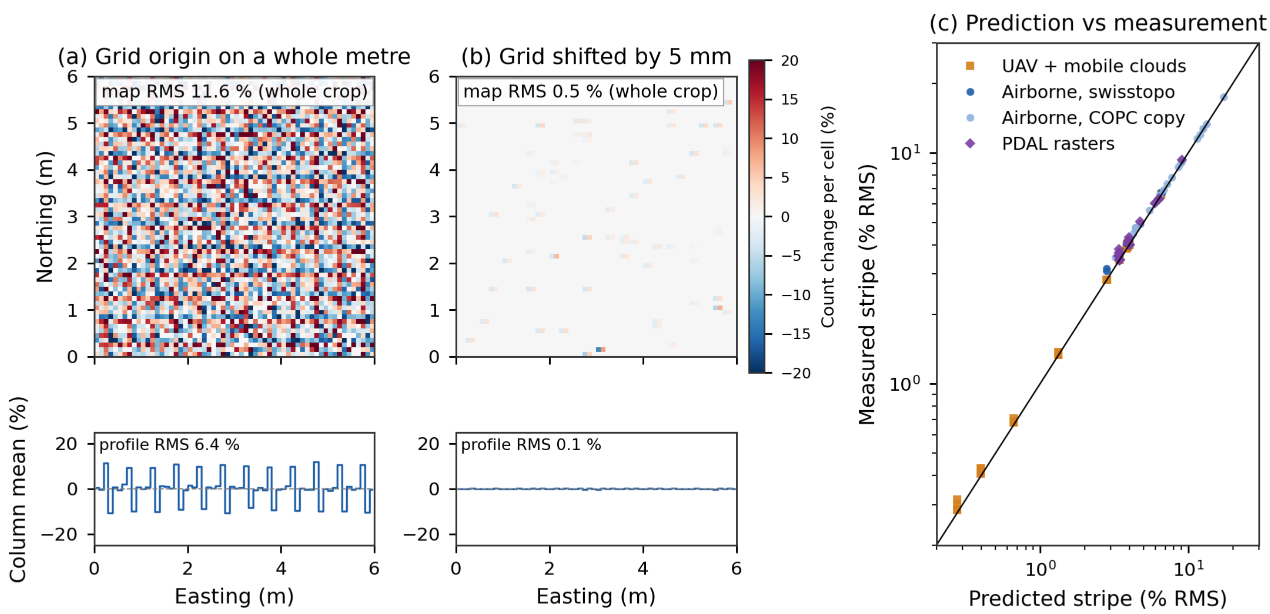


Figure 1: **A regular count pattern from storage, and its removal.** (a) PDAL counts in 0.1 m cells of a UAV crop stored at 1 cm, divided by the counts of the same points from their original 0.1 mm coordinates; grid origin on a whole metre. (b) The same grid shifted by 5 mm. Lower strips: column means of each window (easting profile), which isolate the easting stripe (6.4 % RMS in a, 0.1 % in b); the map RMS also contains the northing stripe and cell-level scatter. Windows are 6 m × 6 m (south-west corner E 516,987 m, N 4,644,807 m, UTM 29N); colours clipped at ±20 %. (c) Predicted against measured one-axis RMS stripe for all real-data tests with a predicted stripe above noise; airborne values are the excess over counting noise.

Petras et al. (2023) described moiré in airborne density rasters and attributed it to the overlap of the sensor's point pattern with the raster grid. The ASPRS density guidelines (ASPRS 2025) show that cell size changes density results. Neither addresses the storage step of the file. We did not re-analyse their data; the bound below limits what storage can contribute to such patterns, and the jitter and recount tests of Table 1 separate the two sources. Aliasing, dither and the square-root growth of signal over counting noise are standard (Widrow and Kollár 2008); counts of rounded data have a long history in statistics (Sheppard 1897; Heitjan 1989). The underlying effect, histogram bins that do not match a quantisation step, is also known from the code-density test for analog-to-digital converters (IEEE 2011). What is new here is its form in LAS files and raster software: the storage step, floating-point cell edges in PDAL and lidR, uneven filling introduced by processing, and a test a user can apply to a given raster.

The effect is largest at fine cells. By Eq. (1) (Section 2.2) the grid-mismatch stripe is at most $q/2c$: 5 % at 10 cm but 0.5 % at 1 m for a 1 cm step. A moiré of several per cent in metre-scale cells therefore cannot come from grid mismatch, while one in decimetre cells could. The effect matters mainly for cells below a few decimetres and for analyses that pool many cells, such as spectra, texture measures and gridded inputs to classifiers.

The investigation grew out of developing OpenLiDARViewer (Urias 2026). Similar patterns observed across several point-cloud tools prompted a closer look at how stored coordinates interact with raster grids. The formal software tests reported here use PDAL and lidR.

Our contribution is a characterisation of how LAS storage spacing and boundary arithmetic produce count-raster patterns, with predicted size, spectral location and detectability, validated on real data and turned into a set of controlled changes that test whether a given pattern came from storage and counting. We organise it around three questions: where should a false pattern appear, how strong should it be, and what controlled change should weaken or move it?

## 2. How counting creates a pattern

A LAS file records positions on a fixed step, as a digital recording samples sound at a fixed rate. A raster that does not divide evenly into that step gives some cells one column more than others, and the difference repeats like a beat between two rates (Eqs. 1–2). A cell edge that sits exactly on a stored position can be rounded to the wrong side by floating-point arithmetic (Section 2.3). And a steady repetition, however small, stands farther above random counting noise as more points are analysed (Eq. 3).

### 2.1 From stored positions to counts

LAS stores each coordinate as an integer $X$ with scale $s$ and offset $o$: $x = o + X \cdot s$ (ASPRS 2019). With the common $s = 0.01$ m, which PDAL writes by default, every stored easting is $o$ plus a whole number of centimetres. We call these permitted positions *columns* and their spacing the *storage step q*. The storage step is a property of the file, not of sensor accuracy or of the spacing between actual points.

We use three quantities and keep them apart. A raster can count the stored coordinates correctly and still carry a pattern: the *stripe* is the periodic departure of counts from their expected value under the occupancy model (Sections 2.2 and 2.4). The *count change* compares counts from 1 cm coordinates with counts of the same points from finer stored coordinates, which serve as a reference, not as ground truth (Fig. 1, twin tests). *Misassignment* is a different problem: points placed in the wrong cell by floating-point arithmetic (Section 2.3). Individual columns may be empty; across many cells, however, the unequal number of available positions produces a predictable average pattern.

## 2.2 Grid mismatch

With q = 1 cm, a 12.5 cm cell cannot contain 12.5 columns (stored positions, not raster columns), so successive cells contain 12 or 13. If the columns are equally filled, counts alternate even over uniform ground (Fig. 2a).

*How large is this, typically?* Write r = c/q for the number of steps per cell and f for its fractional part. A fraction f of cells holds one extra column, and the root-mean-square (RMS) change, a measure of typical error size along one axis, is

$$\mathrm{RMS} = \frac{\sqrt{f(1-f)}}{r} \;\le\; \frac{q}{2c}. \tag{1}$$

Single cells can deviate more than the RMS: at 13.3 cm, cells hold 13 or 14 columns and deviate by −2.26 % or +5.26 %, while the RMS is 3.45 %. A two-dimensional map carries a stripe along each axis. When f = 0 (c a whole multiple of q) this mechanism is absent.

## 2.3 Boundary rounding

Take c = 10 cm, a whole multiple of q. If a boundary falls exactly on a column, software computes the cell index $\lfloor (x - g)/c \rfloor$ in floating point for grid origin g; the result can land just below a whole number, and the column's points go to the neighbouring cell (Fig. 2b). For example, with offset and grid origin both at 2,485,000 m, s = 0.01 m and c = 0.1 m, the stored integer X = 30 decodes to 2,485,000.3 m, and (x − g)/c evaluates to 2.999999998 in float64: the point lands in cell 2 instead of 3. The integer form, X ÷ 10, gives 3. The one-axis RMS change is bounded by q/c (Appendix A).

When c is a whole multiple of q, the remedy is to place boundaries halfway between stored positions: g = o + (m + ½)q for a whole number m, separately for each axis with that axis's offset and scale. This works while accumulated numerical error stays much smaller than the half-step gap: in float64 at coordinates near $10^6$ m, errors are near $10^{-10}$ m; in float32 at $10^6$ m, adjacent values are 0.0625 m apart, so coordinates must be rebased to a nearby origin before conversion to float32 (Goldberg 1991). Computing cell indices from the stored integers with integer arithmetic, as our reference implementation does, avoids the ambiguity:

```python
UM = 10**6  # integer micrometres
def cell_index(X, scale, offset, origin, cell):
    # X: stored LAS integers (numpy int64); other arguments in metres
    num = round(offset*UM) + X*round(scale*UM) - round(origin*UM)
    return num // round(cell*UM)
```

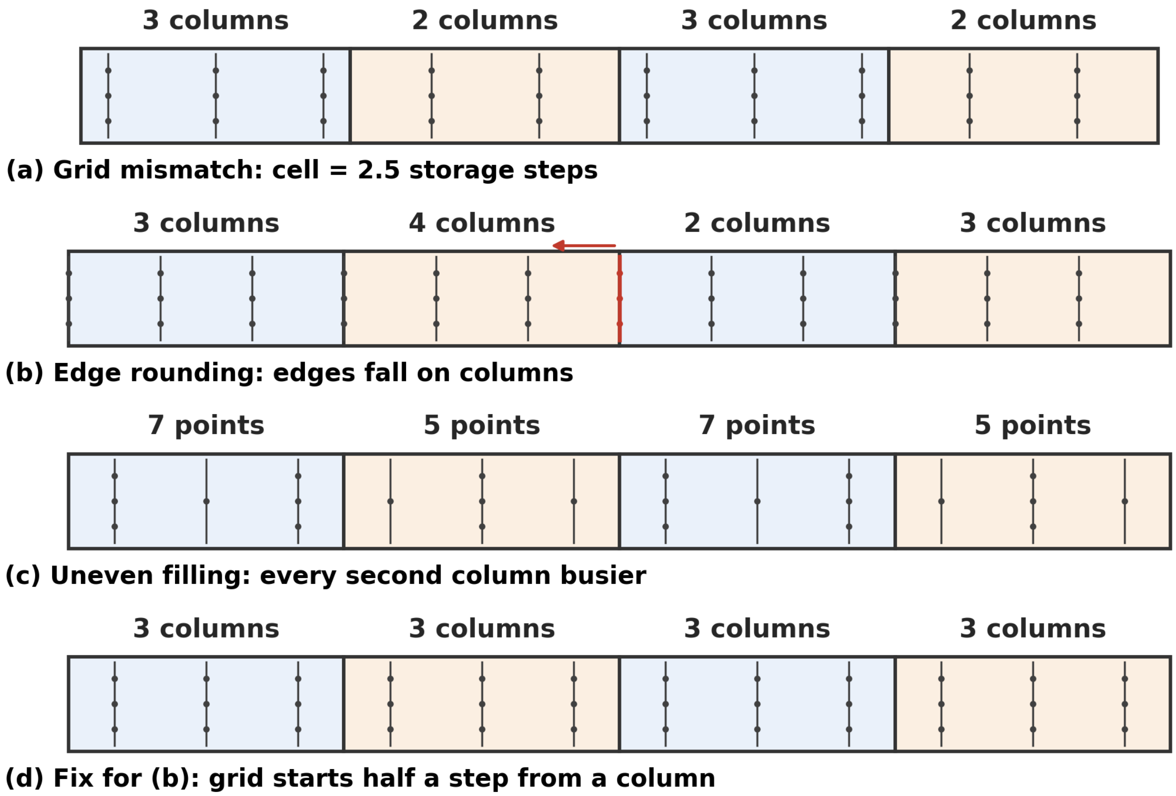


Figure 2: **Three mechanisms, and the fix for the second.** Vertical lines are columns, dots are points. (a) Cells 2.5 steps wide alternate between 2 and 3 columns. (b) Cells 3 steps wide with edges on columns: a column on an edge decodes slightly low and moves one cell left. (c) Every second column holds more points; cells of 3 columns alternately hold 2 or 1 busy column. (d) Boundaries halfway between columns fix (b) only. Remedies: for (a), a cell width that is a whole number of steps; for (b), the half-step origin in (d); for (c), a cell width that is a multiple of the filling pattern (here 2 steps).

## 2.4 Uneven filling

A file's processing history can fill columns unevenly, for example in a pattern repeating every M steps (Fig. 2c). Cells then hold equal numbers of columns but unequal numbers of busy ones, and a grid shift does not help. Cell widths spanning whole patterns (multiples of M·q) remove the ideal periodic part. A histogram of the stored integers modulo a chosen number reveals such a pattern only if that number is compatible with the period; a flat histogram at one modulus does not prove even filling.

### 2.5 From counts to a spectrum

A spectrum measures how strongly a profile repeats at each spacing. *Where does grid mismatch appear?* Its strongest line sits at

$$\nu = \min(f,\, 1 - f) \text{ cycles per cell}, \qquad L = c/\nu \text{ on the ground}, \tag{2}$$

with weaker lines at multiples of f, folded into the range 0 to ½. At 13.3 cm, $\nu = 0.3$ and L = 44 cm; the full count sequence repeats only every 10 cells (1.33 m). For f = 0 there is no line. Eq. (2) needs only c and q; lines from boundary rounding and uneven filling depend also on which edges misfire and on the filling pattern.

*How strong in a spectrum?* A faint, steady note can be difficult to hear in background noise, yet frequency analysis can reveal it; here the repetition runs across distance rather than time. The error can stay the same size while becoming easier to detect. Its line stands above the median of the spectral background by approximately

$$R \approx \frac{A\sqrt{N}}{1.67}, \tag{3}$$

where A is the line amplitude as a fraction of the mean count and N the number of points analysed. At fixed A, four times as many points roughly doubles R. A practitioner can estimate A from Appendix A and N from the data to judge whether a predicted line could stand out. Eq. (3) assumes roughly independent, Poisson-like counting noise; R is a ratio to the background, not a significance level or false-alarm rate. The number of cells does not enter the idealised noise, but enough cells are still needed to resolve the frequency.

*What changes it?* Table 1 lists the controlled change that tests each mechanism.

## 3. Data and methods

**Point clouds.** UAV: DJI Zenmuse L1 vineyard survey (Vélez et al. 2023), 46.8 million points stored at 0.1 mm. Mobile: mapry LA03 forest scan (Hrdina 2025), 31.6 million points at 0.1 mm. Airborne: swisstopo swissSURFACE3D tile 2485-1109, 15.7 million points at 1 cm. Second airborne file: a COPC file for the same tile from a public mirror (Section 4.5).

**Twin binning.** We rounded the UAV and mobile clouds to 1 cm and 1 mm and counted the same points before and after. The ratio removes scene features that vary smoothly across a cell, not sharp features that straddle an edge; we excluded bins whose count differed by more than 50 % from their neighbours (Section 4.3).

**Held-out prediction.** For the airborne files we learned the column filling from one half of the tile and predicted stripes in the other half.

**Spectra.** We measured the amplitude of easting stripe profiles at each predicted frequency (main line and four multiples) and compared it with the predicted profile. Two empirical references were computed from frequencies away from all predicted lines: the median, for Eq. (3), and the 99.9th percentile of 2,000 frequencies, used to say a line stands out. Neither is itself a significance test. For reference, under ideal independent Rayleigh-distributed noise with a known median, the probability that any of 2,000 frequencies exceeds 3.91 times the median is 5 %; our estimated medians from detrended profiles are not calibrated to that model.

**Detectability and moving-line tests.** We randomly thinned the northern half of the airborne tile (7.84 million points) at four cell sizes, which changes N inside a fixed footprint, and recounted the UAV points along easting at eight cell sizes (10.75 to 17.45 cm, f between 0.3 and 0.75), tracking the strongest line in the 1 cm spectrum and a reference component in a fixed 3.3 to 3.9 m window (Appendix B).

**Software.** PDAL 2.10.2 (`writers.gdal`, `output_type` count, `binmode` true; Butler et al. 2021; PDAL Contributors 2025) and lidR 4.3.3 (`pixel_metrics`; Roussel et al. 2020) rasterised a 40 m UAV crop rounded to 1 cm by PDAL (offset 0) and a 400 m crop of the swisstopo tile (offsets 2,485,000 and 1,109,000 m), with the origin on a whole metre, a whole metre plus 5 mm, or each program's default. We regressed measured on predicted stripes bin by bin; a slope of 1 means the prediction has the right size. Appendix B gives the protocol and Appendix C maps each claim to its script and result file.

# 4. Results

## 4.1 Hidden in the map, visible in the spectrum

In the airborne tile a single cell has a stripe-to-noise ratio near 0.03, so the stripe is far below the counting noise of any one cell. Its easting profile shows the predicted lines (Fig. 3a). Across seven cell sizes the main lines reached 4.6 to 22 times the 99.9th-percentile level. Jittering each coordinate within ±0.5 cm reduced each tested grid-mismatch line 5- to 400-fold, below that reference level. Lines from the file's 25 cm filling pattern remained, at up to twice the level, as expected for uneven filling.

Thinning tested Eq. (3) (Fig. 3b). For the 159 cases with predicted $R \geq 3$ (N from about 17,000 to 7.8 million), a log–log regression of measured R on predicted R gave a slope of 1.03 (expected 1), with a median measured-to-predicted ratio of 0.97. We do not report an interval: the four cell sizes reuse the same points, so cases are not independent. Regressing log R on log N separately for each cell size gave slopes of 0.50 to 0.53 (expected 0.5). Below about 10,000 points the lines were not separable from the background. In these conditions the predicted $R = 5$ fell at 34,000 to 66,000 points and the thinned profiles first reached a median of 5 at 36,000 to 78,000. The median background matched the Poisson prediction within −8 % to +23 % after thinning and

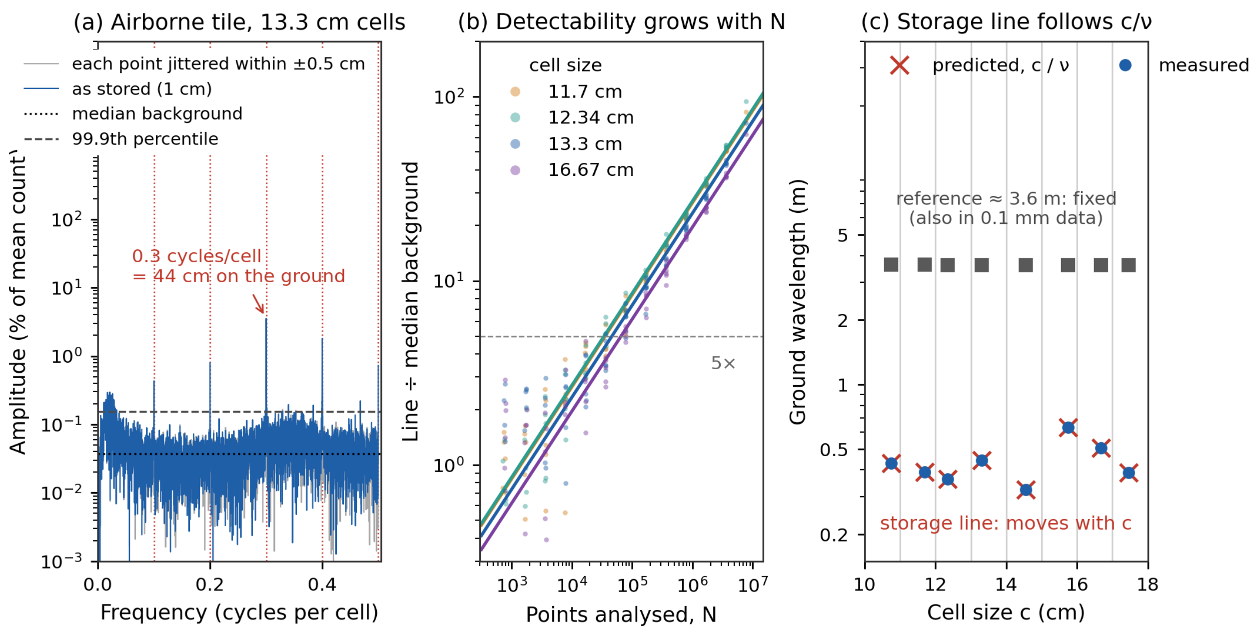


Figure 3: **A pattern hidden in the map is visible in the spectrum, grows with the number of points and moves with cell size.** (a) Airborne easting spectrum at 13.3 cm, as stored and jittered within ±0.5 cm; vertical dotted lines mark multiples of $\nu = 0.3$; horizontal lines show the median and 99.9th percentile of off-line amplitudes in this spectrum. (b) Line height above the median background, R, against points analysed after random thinning, at four cell sizes; lines are Eq. (3) without fitting. (c) Ground wavelength of the strongest line in the 1 cm UAV spectrum (dots), its prediction $c/\nu$ (crosses) and a reference component tracked near 3.6 m (squares), at eight cell sizes; grey lines mark whole-centimetre cells, where the grid-mismatch line is absent.

lay 10 to 20 % below it at full density, which suggests that airborne sampling is more regular than random; at full density Eq. (3) therefore slightly underestimates R.

## 4.2 The storage line follows its prediction

At all eight cell sizes the strongest line in the 1 cm UAV spectrum sat at the predicted wavelength $c/\nu$ within one frequency bin, moving between 32 and 63 cm (Fig. 3c). It measured 2.9 % to 4.5 % after rounding and 0.04 % to 0.19 % at the same frequency in the 0.1 mm data. The reference component stayed at 3.60 to 3.62 m with nearly the same amplitude in both versions (0.95 % to 1.08 %). It is present in the 0.1 mm data, so it does not come from 1 cm storage. The strongest periodic structure in the native two-dimensional count map has a spacing of 1.73 m with its normal 153° from east, probably the vine rows; its trace along easting falls at 1.95 m, so the rows do not account for the 3.6 m component. Flight-line overlap and the scan pattern were not tested. It was tracked in a fixed window that never overlapped a storage line. Agreement with the predicted movement supports a storage origin for the moving line. Other peaks may still come from storage or resampling, especially where peaks overlap. The mobile scan was not used for this test because its own 0.1 mm coordinates are unevenly filled: one stored value in every ten holds 38 % more points than average, so its native spectrum already carries storage lines.

## 4.3 Sizes and lines match the predictions

Exact column counts matched Eq. (1) in 1,200 synthetic grids to within $9.3 \times 10^{-16}$ (Fig. 5a). In real data (n = number of conditions; twin binning at 1 cm and 1 mm):

| Test | Prediction from | n | Slope, median (range) | $R^2$, median (range) |
|---|---|---|---|---|
| Twin binning, UAV and mobile | exact column counts | 40 | 1.00 (0.99–1.02) | 0.99 (0.76–1.00) |
| swisstopo tile, held-out | filling of other half | 12 | 1.00 (0.99–1.01) | 0.54 (0.44–0.70) |
| Second public file, held-out | filling of other half | 20 | 1.00 (0.99–1.01) | 0.82 (0.56–0.93) |
| PDAL rasters, all origins | exact counts, float64 edges | 29 | 1.00 (0.96–1.04) | 0.99 (0.44–1.00) |

$R^2$ is lower in the airborne rows because counting noise, not error in the prediction, dominates those profiles. The twin result depends on the exclusion rule in two conditions. Without it, 38 of 40 conditions were unchanged, but mobile easting at 12.34 and 13.3 cm gave slopes of 5.0 and 5.8 with $R^2$ below 0.01, because 1.39 million points of a vertical structure fall within 13 cm straddling a cell edge. The rule drops bins whose original-coordinate count differs by more than 50 % from the mean of their two neighbours (median 0.05 % of bins, at most 7.5 %). With it, those conditions gave 1.00 and 1.00 ($R^2$ 0.99 and 0.98). The same mask was applied to measured and predicted profiles, which retained close agreement after masking (Fig. 4a). The mask removed three bins in each condition and changed the predicted main-line amplitude by less than 1 % (from 2.54 % without the mask to 2.52 % with it at 12.34 cm, and from 2.25 % to 2.24 % at 13.3 cm); without it, the unmasked edge spike raised the measured amplitude to 14.9 % and 14.3 %, a broadband contribution from one structure rather than a storage line.

We tested 79 spectral lines in 23 profiles: 75 grid-mismatch lines and four uneven-filling lines of the two airborne files at 5 cm. All 75 grid-mismatch lines exceeded the 99.9th-percentile level, and amplitudes were 0.90 to 1.09 times the predictions (Fig. 4a). Because they come from shared profiles, the 79 lines are repeated checks of one model on the same data. In a two-dimensional spectrum of the UAV twin ratio, the main lines measured 3.65 % and 3.63 % against 3.59 % and 3.58 % predicted (Fig. 5c). Eq. (A3) also held in single count maps of the UAV crop, with no twin reference: the stripe was fitted to the predicted pattern and the counting noise was measured from the difference of two random halves of the points. Over densities from 46 to 4,600 points per m² at 12.5 and 13.3 cm, the observed stripe-to-noise ratio (0.05 to 0.49) was 0.97 to 1.08 times the prediction (log–log slope 0.99; Fig. 5b), and the measured noise matched the Poisson value within 1 %.

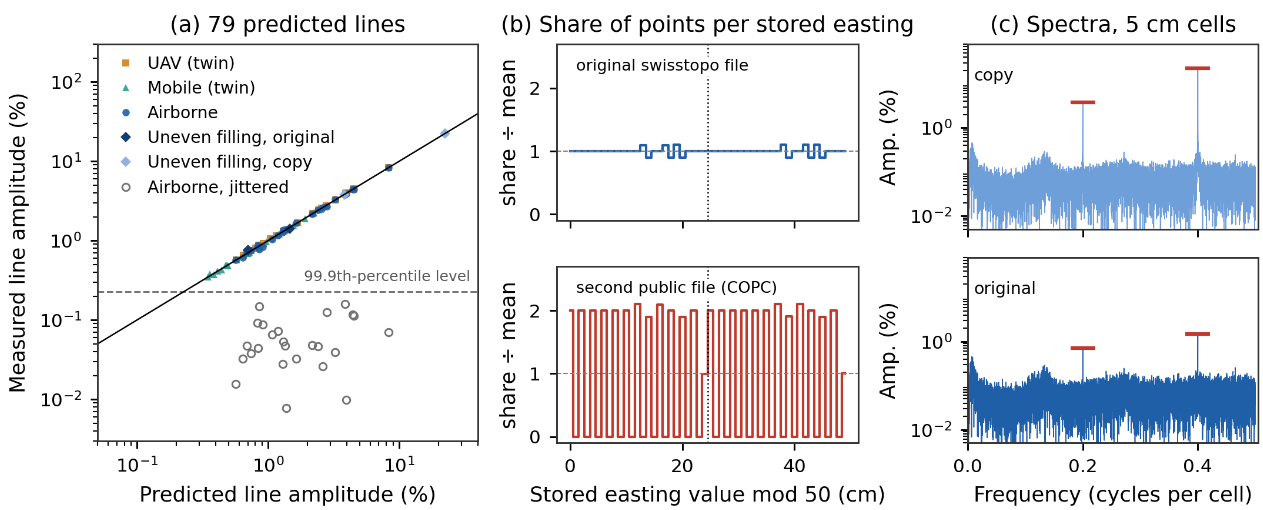


Figure 4: **Predicted and measured lines, and two public files for the same tile.** (a) Measured against predicted amplitude for 79 lines; open circles are the jittered airborne control, dashed line the median airborne 99.9th-percentile level. (b) Share of points per stored easting value, modulo 50 cm, in the swisstopo file (top) and the second public file for the same tile (bottom); 1 means even filling, and the dotted line marks the 25 cm shift of the pattern. (c) Easting spectra of both at 5 cm; red bars are predictions from column filling learned on the other half of the tile.

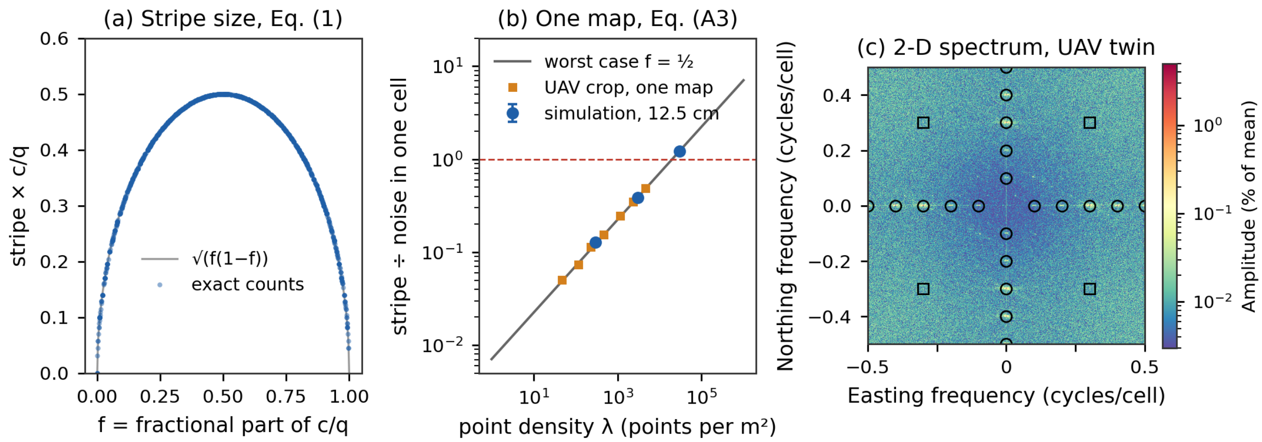


Figure 5: **Checks of the size law and its two-dimensional form.** (a) Exact column counts in 1,200 synthetic grids against Eq. (1). (b) Single-map stripe-to-noise ratio for a 1 cm step at f = ½ (Eq. A3): Poisson simulations and single maps of the UAV crop at 12.5 cm, thinned to lower densities. (c) Two-dimensional spectrum of the UAV twin ratio at 13.3 cm; circles mark predicted axis lines, squares the weak cross terms.

## 4.4 Boundary rounding in PDAL and lidR

With float64 and the origin on a column, synthetic binning misplaced at least one column in 68 % to 71 % of configurations with 5, 10 and 20 cm cells, and in 5 % to 7 % with 25, 50 and 100 cm cells. Half-step origins removed every misplacement in 24,000 configurations. PDAL at 10 cm with the origin on a whole metre produced 6.3 % stripes on the UAV crop, against 6.3 % predicted by Eq. (A2). The misfire share and neighbour correlation in that prediction ($p = 0.20$, $\rho = -0.25$) came from evaluating the same float64 arithmetic at each on-column edge before rasterising. On the airborne crop the stripes were 6 % to 9 % above noise. The 5 mm shift brought both to noise level and left the 12.5 and 13.3 cm grid-mismatch stripes unchanged. PDAL's default easting origin fell on a UAV column and produced the stripe; its other defaults fell nanometres off columns and did not misfire. lidR's default grid produced the stripe along easting (6.3 % UAV; 7.3 % against 4.0 % noise airborne), and a 5 mm shift of `start` removed it.

For grid mismatch in lidR, stripe magnitudes on the UAV crop (3.4 % to 4.1 %) matched Eq. (1), and 12 of 16 conditions gave slopes of 0.95 to 1.03. Four conditions at 13.3 cm gave 0.64 to 0.88. There the stripe size matched but the predicted and measured profiles were misaligned. We could not reproduce lidR's exact floating-point cell edges, which is a likely but unverified cause. Because the stripe sizes matched, the tests in Table 1 are unaffected.

## 4.5 Uneven filling: two public files for the same tile

The swisstopo file fills its columns almost evenly (0.90 to 1.10 of the average share). A second public file for the same tile, distributed as COPC, has the same point count and generating-software field but a different pattern (Fig. 4b): along easting only every second centimetre is used, shifting every 25 cm; along northing one value is skipped and another doubled in each 25 cm block. Both patterns can be reproduced exactly from the original file. Snapping each stored easting down to a 2 cm grid that restarts at every 25 cm block, and mapping each northing position r within a 25 cm block to round(24r/25), turns the original coordinates into the second file's coordinates: the sorted easting and northing values of the transformed original equal those of the second file, value for value, over all 15.7 million points. This matches the marginal coordinates, not individual points, and does not identify the software that applied it. Converting the original file with PDAL 2.10.2 (`writers.copc`, default settings) left every stored coordinate unchanged, so COPC encoding alone does not produce the pattern; users of redistributed copies can detect such a change from the stored-integer histogram before rasterising. The second file shows stripes up to 18 % at 5 cm cells (17.5 % above counting noise), where the original shows none above noise; the filling model predicted them (slopes 0.99 to 1.01) and its lines at 0.2 and 0.4 cycles per cell (3.8 % and 22.5 % measured, 3.8 % and 22.4 % predicted; Fig. 4c). At 25 and 50 cm cells, multiples of the 25 cm pattern, both files gave the same RMS (2.7 % along easting).

### 4.6 Ratios

A distortion that multiplies numerator and denominator about equally cancels in their ratio. For ground fraction on the swisstopo tile at 12.5 cm, the predicted stripe fitted point counts with slope 1.005 but ground fraction with slope −0.007 [−0.024, 0.010]; the stripe appeared in absolute counts and was absent from this ratio. Ratios whose parts are filled differently are not protected.

## 5. A diagnostic

**Table 1.** Controlled changes that test a suspected storage pattern. "Tested" marks responses observed here; the rest follow from the model.

| If you suspect | Change | You should observe | You can conclude |
|---|---|---|---|
| Grid mismatch | Recount at another cell size | Peak moves to the new $L = c/\nu$ (tested) | Moving peak: storage; fixed L: not grid mismatch |
| Grid mismatch | Jitter coordinates by up to $\pm q/2$ | Grid-mismatch lines drop below background (tested) | Lines came from storage columns; a test, not a fix |
| Boundary rounding | Boundaries halfway between stored positions (c a multiple of q) | Stripe disappears (tested, PDAL, lidR) | Edges sat on stored positions; to keep an existing grid, index on integers |

| If you suspect | Change | You should observe | You can conclude |
|---|---|---|---|
| Uneven filling | Cells spanning whole filling periods, M·q | Periodic part disappears (tested, 25 and 50 cm) | Pattern follows the filling; coarser cells cost resolution |
| Any | Compare counts with a ratio of counts | Stripe in counts, not ratio (tested, ground fraction) | Distortion multiplies both counts alike |

Different responses point to different sources, but the table is not a validated classifier and several mechanisms can coexist.

### 5.1 Limitations

The tests used point counts from three platforms (UAV, mobile and airborne) and two programs (PDAL and lidR). Elevation statistics, the vertical axis, voxel grids and radius-based gridding were not tested. The moving-line and 2-D tests used a single UAV survey, and the physical origin of the reference component near 3.6 m is unknown. Thinning changed N within one footprint, so it does not show that the same scaling holds for larger areas, additional flight lines or mixed scenes. Eq. (A3) was tested on one UAV crop at up to 4,600 points per m², below the density of about 20,000 points per m² at which a single map shows the stripe at the noise level. We found no published case in which a storage line was read as a real feature.

## 6. Conclusion

A LAS file permits coordinates only at fixed positions, and a raster counts the points in each cell. Incompatible spacing, boundary arithmetic or uneven filling turn that into regular count differences, which a spectrum can reveal even when a map cannot. The second public swisstopo file shows that a different stored-coordinate pattern can change the raster: a simple transformation of the original file reproduces its coordinate marginals exactly, and the file has stripes of up to 18 % that the original does not show. Because each mechanism responds to a different controlled change, a suspicious pattern can be tested rather than guessed at.

## Acknowledgements

The author identified the problem while developing OpenLiDARViewer (Urias 2026) and designed and ran all tests. Parts of the code and text were drafted with Claude (Anthropic) and revised by the author. The work received no external funding.

## Data and code availability

- UAV survey: CC BY 4.0, doi:10.5281/zenodo.8113105 (20220714_FLEXI-GROBOTS_L1_PRO_20M_4MS_B9.laz).
- Mobile scan: CC BY 4.0, doi:10.5281/zenodo.15421291 (LA03mapry.laz).
- swissSURFACE3D tile 2485-1109: © swisstopo, data.geo.admin.ch (item swisssurface3d_2019_2485-1109).
- Second public file: https://open-lidar-data.s3.eu-central-1.amazonaws.com/data/CH/Swiss_federal_authorities/swisssurface3d_2022/copc/2485_1109.copc.laz.
- Analysis code, pipelines and result files for this study: Zenodo, doi:10.5281/zenodo.22969166. This archive is separate from the OpenLiDARViewer software.

## References

ASPRS. 2019. *LAS Specification 1.4 – R15*. Bethesda, MD: ASPRS.

ASPRS. 2025. *ASPRS Guidelines on Quantifying Horizontal Sampling Density of Aerial Lidar Point Cloud Data*. Edition 1, Version 1.0. Bethesda, MD: ASPRS.

Butler, H., B. Chambers, P. Hartzell, and C. Glennie. 2021. “PDAL: An Open Source Library for the Processing and Analysis of Point Clouds.” *Computers & Geosciences* 148: 104680. doi:10.1016/j.cageo.2020.104680.

Goldberg, D. 1991. “What Every Computer Scientist Should Know about Floating-Point Arithmetic.” *ACM Computing Surveys* 23 (1): 5–48.

Heitjan, D. F. 1989. “Inference from Grouped Continuous Data: A Review.” *Statistical Science* 4 (2): 164–179.

Hrdina, M. 2025. “LiDAR Scanners Comparison – Point Clouds.” Zenodo. doi:10.5281/zenodo.15421291.

IEEE. 2011. *IEEE Standard for Terminology and Test Methods for Analog-to-Digital Converters*. IEEE Std 1241-2010. New York: IEEE. doi:10.1109/IEEESTD.2011.5692956.

Lothaire, M. 2002. *Algebraic Combinatorics on Words*. Cambridge: Cambridge University Press.

PDAL Contributors. 2025. *PDAL Point Data Abstraction Library*. Zenodo. doi:10.5281/zenodo.10884408.

Petras, V., A. Petrasova, J. B. McCarter, H. Mitasova, and R. K. Meentemeyer. 2023. “Point Density Variations in Airborne Lidar Point Clouds.” *Sensors* 23 (3): 1593. doi:10.3390/s23031593.

Roussel, J.-R., D. Auty, N. C. Coops, P. Tompalski, T. R. H. Goodbody, A. Sánchez Meador, J.-F. Bourdon, F. de Boissieu, and A. Achim. 2020. "lidR: An R Package for Analysis of Airborne Laser Scanning (ALS) Data." *Remote Sensing of Environment* 251: 112061.

Sheppard, W. F. 1897. "On the Calculation of the Most Probable Values of Frequency-Constants, for Data Arranged According to Equidistant Division of a Scale." *Proceedings of the London Mathematical Society* s1-29 (1): 353–380. doi:10.1112/plms/s1-29.1.353.

Urias, A. 2026. *OpenLiDARViewer*. Version 0.6.9. Software. Zenodo. doi:10.5281/zenodo.22821525. Source code: https://github.com/Aurtechmx/openlidarviewer.

Vélez, S., M. Ariza-Sentís, and J. Valente. 2023. "High Resolution LiDAR Dataset Acquired Using UAV (Unmanned Aerial Vehicle) over Two Vineyards and Two Years Located in 'Tomiño', Pontevedra, Spain." Zenodo. doi:10.5281/zenodo.8113105.

Widrow, B., and I. Kollár. 2008. *Quantization Noise*. Cambridge: Cambridge University Press.

## Appendix A. Derivations

**Line amplitudes.** The column count of cell $j$ is $n_j = \lfloor (j+1)r + \varphi \rfloor - \lfloor jr + \varphi \rfloor$, a mechanical (Sturmian) sequence (Lothaire 2002). Writing each floor as its argument minus a periodic sawtooth and expanding in sines gives lines at $\nu_k = kf \bmod 1$, folded into $[0, \frac{1}{2}]$, with amplitude

$$A_k = \frac{2\,|\sin(\pi k f)|}{\pi k r}, \qquad \tfrac{1}{2} \sum_{k \geq 1} A_k^2 = \frac{f(1-f)}{r^2}. \tag{A1}$$

Frequencies are exact. Amplitudes are exact for irrational $f$ over an infinite sequence; for $f = a/b$ the sequence repeats every $b$ cells, lines that fold onto one frequency add as phasors, and we therefore predict each line from exact column counts. Finite windows spread each line slightly across neighbouring frequencies. At $\nu = \frac{1}{2}$ (Nyquist) we report $|Z|$ without the factor 2; for $f = \frac{1}{2}$ the counts alternate with amplitude $1/(2r)$. Uneven filling with period $M$ adds lines at multiples of $c/(Mq)$ and their sums and differences with $kf$. In two dimensions the product of the axis stripes adds cross terms at $(\pm\nu_x, \pm\nu_y)$ with amplitude $A_x A_y/2$; for the UAV window this gives 0.064 %, against 0.07 % from exact counts and 0.08 to 0.10 % measured.

**Boundary rounding.** If a share $p$ of on-column edges misfire, with correlation $\rho$ between neighbours,

$$\text{RMS} = \frac{\sqrt{2p(1-p)(1-\rho)}}{r} \;\leq\; \frac{q}{c}. \tag{A2}$$

**One map.** A cell expecting $\lambda c^2$ points ($\lambda$ = point density) has Poisson noise $1/(c\sqrt{\lambda})$. Adding the two axis stripes and neglecting their product (first order, valid while both are small) gives the stripe-to-noise ratio

$$S = q\sqrt{2\lambda f(1-f)} \ \leq \ q\sqrt{\lambda/2}. \tag{A3}$$

$S = 1$ at $\lambda = 1/[2q^2 f(1-f)]$: 20,000 points per m² for $q$ = 1 cm at $f = \frac{1}{2}$ under this model; other $f$ need more.

**Detectability.** A profile of $n$ bins holding $N$ points has relative Poisson noise $\sigma = \sqrt{n/N}$ per bin. At an ordinary frequency (not 0 or Nyquist) the coefficient $Z = \frac{1}{n}\sum_j d_j e^{-2\pi i\nu j}$ of white noise has $\mathrm{E}|Z|^2 = \sigma^2/n$, so $2|Z|$ is Rayleigh-distributed with median

$$\frac{1.665\,\sigma}{\sqrt{n}} = \frac{1.665}{\sqrt{N}}, \qquad R = \frac{A\sqrt{N}}{1.665}. \tag{A4}$$

## Appendix B. Protocol

**Binning.** Grid-mismatch tests used exact integer binning (integer micrometres) so that boundary rounding could not contribute. Slopes come from ordinary least squares, bin by bin, with 95 % moving-block bootstrap intervals (blocks of 20 bins, 2,000 resamples, seed 0).

**Held-out.** Column weights (period 100) from the half south or west of the median; test on the other half; terrain removed by a moving average of max(31 cells, 8 m); predicted stripes reported above 0.02.

**Spectra.** Line amplitude is $2|Z|$ with $Z$ as defined in Appendix A ($|Z|$ at $\nu = \frac{1}{2}$). Twin profiles: ratio minus one, excluded bins set to zero in measured and predicted profiles. Airborne: northern half, weights from the southern half, same detrending for prediction and data. 99.9th-percentile level: 2,000 frequencies in 0.06–0.49 cycles per cell, ≥ 0.01 from lines k = 1–8 and filling lines; close to the second-largest value. 79-line slope 0.998 [0.991, 1.005], resampling whole profiles (4,000, seed 0). Jitter seeds 3 and 4. 2-D test: 600 × 600 cells of 13.3 cm (E 516,950, N 4,644,775), cells with ≥ 20 native points (91 %).

**Detectability.** 13 thinning levels $10^{-4}$ to 1; five draws below 1; seed 11; cells 11.7, 12.34, 13.3 and 16.67 cm; median background at 0.06–0.49 cycles per cell away from lines k = 1–8, Nyquist bin excluded. Slope 1.03 over 159 cases with predicted R ≥ 3 (log measured R on log predicted R); no interval reported because cell sizes share points.

**Moving-line.** Whole UAV cloud, origin on a whole metre; one frequency bin ≈ 0.11 m at 3.6 m.

**Synthetic Eq. (A1) test.** 400,000 cells at $r = 12 + (\sqrt{5} - 1)/2$, $11 + \sqrt{2}$, $4 + \pi$ and $18 + e$ (≈ 12.618, 12.414, 7.142, 20.718), evaluated in double precision: amplitudes matched Eq. (A1) within 0.01 %. Three rational cases were run with the same code: at $r = 12.3$ ($f = 0.3$) the measured-to-formula ratio was 1.02 for $k = 1$ and up to 1.32 for $k = 4$; $r = 12.05$ ($f = 0.05$) gave 1.00 to 1.11; at $r = 12.5$ ($f = ½$) all odd lines fold onto one frequency, so only the combined line (amplitude $1/(2r)$) is meaningful.

**Software.** PDAL cell index $\lfloor(x - g)/c\rfloor$ (`Raster.hpp`); default origins read from the GeoTIFF. lidR columns $\lfloor(x - x\_min)/c\rfloor$, rows $\lfloor(y\_max - y)/c\rfloor$ with floating-point bounds. Python 3.14, numpy, scipy, laspy 2.7; R 4.5 with lidR 4.3.3 and terra 1.9.

**Input files (SHA-256, first 16 hex digits).** UAV 03f4604890636085; mobile 12a56908deea1b74; swisstopo LAS, unzipped, d56bc92c42ce3f4a; second file e41e7e6347b1c7bd.

## Appendix C. Claims, scripts and results

All paths are relative to the analysis archive; each script writes the named result file; the reported outputs are in `results/`. Input SHA-256 hashes are in `INPUT_SHA256.txt`; run order is in `README.md`.

| Claim | Script | Result file |
|---|---|---|
| Fig. 1; PDAL slopes and defaults | `expI.py`, `expM.py`, `anaM.py`, `anaM2.py`, `expN.py`, `figs4.py` | `results_I.json`, `results_M.json`, `results_M_decomp.json`, `results_M_decomp2.json`, `results_N.json` |
| Eq. (1) exact; edge alignment | `expJ.py`, `expE.py` | `results_J.json`, `results_E.json` |
| Boundary misfires; 24,000 half-step configurations; Eq. (A3) simulation | `expF.py` | `results_F.json` |
| Eq. (A3) on single real maps | `expV.py` | `results_V.json` |
| Twin slopes; exclusion effect | `expK.py`, `expK_noexcl.py`, `expMask.py` | `results_K.json`, `results_K_noexcl.json`, `results_mask.json` |
| Held-out slopes; second file; ratio | `expL.py` | `results_L.json` |
| Second file reproduced from the original; COPC conversion test | `expW.py`, `expCOPC.py` | `results_W.json`, `results_copc.json` |
| lidR | `tools/lidr.R`, `expO.py` | `results_O.json` |

| Claim | Script | Result file |
|---|---|---|
| 79 lines; jitter | expQ.py, expQ2.py, anaQ.py | results_Q.json, results_Q2.json, results_Q_summary.json |
| 2-D spectrum | expS.py | results_S.json |
| Detectability | expT.py, anaT.py | results_T.json, results_T_summary.json |
| Moving line; native 2-D scene peak; mobile filling | expU.py, anaMobileFill.py | results_U.json, results_mobile_fill.json |
| Eq. (A1) synthetic | expR.py | results_R.json |
| Figs. 2–5 | fig_schematic.py, figs_main.py, anaHist.py | figure files, results_hist.json |
| Whole chain | run_all.sh, check_inputs.py, tools/pdal_rasters.sh | all of the above |